

Latent Video Diffusion Models for High-Fidelity Video Generation with Arbitrary Lengths

Yingqing He¹ Tianyu Yang² Yong Zhang² Ying Shan² Qifeng Chen¹

¹The Hong Kong University of Science and Technology ²Tencent AI Lab

Abstract

AI-generated content has attracted lots of attention recently, but photo-realistic video synthesis is still challenging. Although many attempts using GANs and autoregressive models have been made in this area, the visual quality and length of generated videos are far from satisfactory. Diffusion models (DMs) are another class of deep generative models and have recently achieved remarkable performance on various image synthesis tasks. However, training image diffusion models usually requires substantial computational resources to achieve a high performance, which makes expanding diffusion models to high-dimensional video synthesis tasks more computationally expensive. To ease this problem while leveraging its advantages, we introduce lightweight video diffusion models that synthesize high-fidelity and arbitrary-long videos from pure noise. Specifically, we propose to perform diffusion and denoising in a low-dimensional 3D latent space, which significantly outperforms previous methods on 3D pixel space when under a limited computational budget. In addition, though trained on tens of frames, our models generate videos with arbitrary lengths, i.e., thousands of frames, in an autoregressive way. Finally, we further introduce conditional latent perturbation to reduce performance degradation during generating long-duration videos. Extensive experiments on various datasets and generated lengths suggest that our framework is able to sample much more realistic and longer videos than previous approaches, including GAN-based, autoregressive-based, and diffusion-based methods.

1. Introduction

A video can provide more informative, attractive, and immersive visual content that presents the physical 3D world. A powerful video generation tool can benefit novel content creation, gaming, and movie production. Thus, rendering photorealistic videos is a long-standing and exciting goal of the computer vision and graphics research community. However, the high-dimensional video samples and

the statistical complexity of real-world video distributions make video synthesis quite challenging and computationally expensive. The synthesizing quality is also far from satisfactory, which limits its real-world applications.

Existing works capitalize on different types of generative models including GANs [2, 25, 26, 29, 34, 35, 39], VAEs [7, 43], autoregressive models [6, 21, 41], and normalizing flows [17]. Particularly, GANs have achieved great success in image generation [1, 14–16], thus extending it to video generation with a dedicated temporal design achieves outstanding results [29, 34]. However, GANs suffer from mode collapse and training instability problems, which makes GAN-based approaches hard to handle complex and diverse video distributions. Besides, many GAN-based methods usually assume that different frames share similar content in a video, which limits the ability to produce videos with novel content emerging over time [29, 34]. Recent GAN-based methods attempt to exploit implicit neural representations of GANs [29, 44], which encounter the problem of periodic motion and performance degradation across time. Most recently, TATS [6] proposes an autoregressive approach that leverages the VQGAN [5] and transformers to synthesize long videos. However, the generation fidelity and resolution still have much room for improvement.

To overcome these limitations, we leverage diffusion models (DMs) [9], another class of generative models that achieve impressive performance in various image synthesis tasks [4, 18, 22–24]. However, directly extending DMs to video synthesis requires substantial computational resources [12, 38]. Thus, we aim to leveraging the powerful representation ability of diffusion models while maintaining a reasonable computing budget for video synthesis. We achieve this by projecting videos to the latent space via a 3D autoencoder and performing denoising and diffusion processes in this low-dimensional space. In addition, to generate long-range videos, we introduce conditional latent prediction and interpolation diffusion models that can extend videos to arbitrary lengths in an autoregressive and hierarchical manner. We further propose conditional latent perturbation, which are pivotal for slowing the performance degradation over time. Ultimately, our framework surpasses

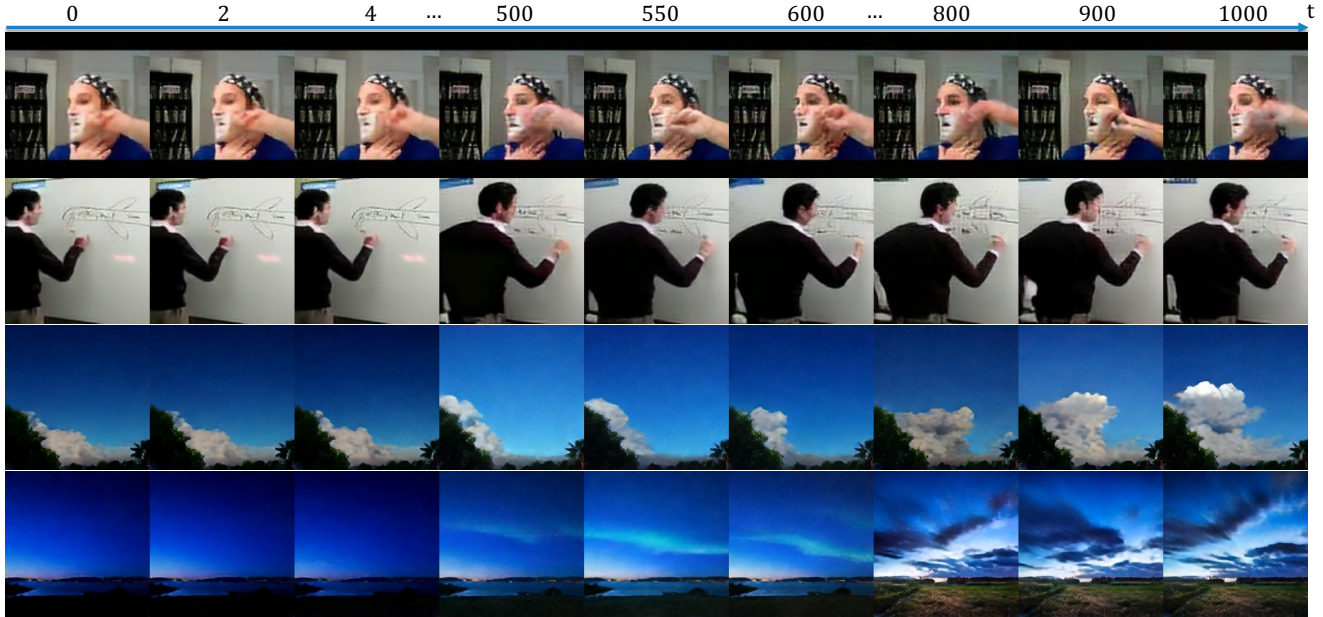


Figure 1. Unconditional video generation results from LVDM with 1000 frames in resolution 256×256 trained on UCF-101 [33] and Sky Time-lapse [42]. LVDM is trained on tens of frames while can generalize to sample arbitrary lengths of videos. Our novel framework can handle long-term diversity while keeping smooth motion transitions. More samples are provided in the supplement.

many previous works in short and long video generation and establishes new state-of-the-art performance on multiple video generation benchmarks.

In sum, our work makes the following contributions:

- We introduce LVDM, a novel and efficient diffusion-based framework for video synthesis, which can jointly perform unconditional generation, autoregressive self-extension, and hierarchical interpolation, facilitating rendering arbitrary-long videos.
- We propose a new latent space normalization for training effective latent-based diffusion models.
- We design a *conditional latent perturbation* technique for autoregressive diffusion models, which distinctly mitigates the problem of quality degradation during long video generation.
- We achieve state-of-the-art results on three datasets and both short and long video generation, demonstrating the effectiveness of our method.

2. Related Work

2.1. Video Synthesis

Video synthesis aims to model the distribution of real-world videos, and then one can randomly draw realistic and novel video samples from the learned distribution. Prior works mainly exploit deep generative models, including GANs [25, 26, 29, 34, 35, 39, 44], autoregressive

models [6, 43], VAEs [7, 40], and normalizing flows [17]. Among them, the most dominant ones are GAN-based approaches due to the great success of GANs in image modeling. MoCoGAN [35] and MoCoGAN-HD [34] learn to decompose latent codes into two subspaces, i.e., content and motion. MoCoGAN-HD [34] leverages the powerful pre-trained StyleGAN2 as the content generator, demonstrating higher-resolution video generation results. StyleGAN-V [29] and DiGAN [44] introduce implicit neural representation to GANs for modeling the continuity of temporal dynamics. They built long-video GAN on top of StyleGAN3 and apply hierarchical generator architecture for long-range modeling, thus producing videos with new content arising in time. Despite these achievements made by GANs, those methods tend to suffer from mode collapse and training instability. Autoregressive methods have also been exploited for video generation. VideoGPT [43] uses VQVAE [20] and transformer to autoregressively generate tokens in a discrete latent space. TATS [6] changes the VQVAE [20] to a more powerful VQGAN [5] and combines a frame interpolation transformer to render long videos in a hierarchical manner. Different from the aforementioned methods, we study diffusion models for video generation in this work.

2.2. Diffusion Models

Diffusion models are a class of likelihood-based generative models that have shown remarkable progress in image synthesis tasks. Due to their desirable properties like stable training and easy scalability, diffusion models have

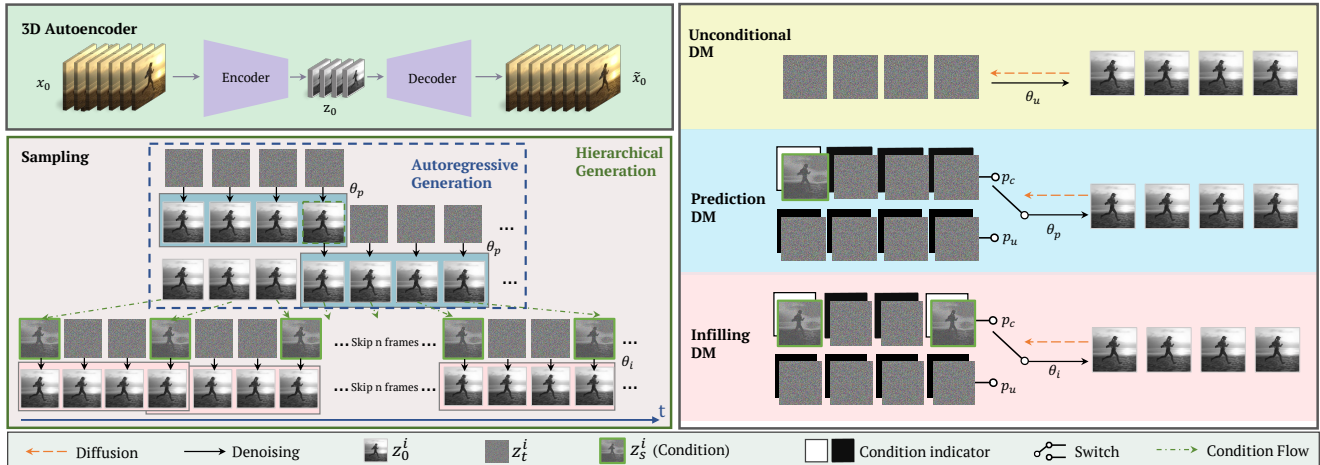


Figure 2. **Framework overview.** We present LVDM, a novel diffusion model (DM)-based framework for video generation. The diffusion and denoising process is performed on the video latent space, which is learned by a *3D autoencoder*. Then an *unconditional DM* is trained on the latent space for generating short video clips. To extend videos to arbitrary lengths, we further propose two frame-conditional models, including a *prediction DM* and an *infilling DM* which can synthesize long-duration videos in autoregressive and hierarchical ways. We utilize noisy conditions at diffusion timestep s to mitigate the condition error induced during the autoregressive sampling process. The frame-conditional DMs are jointly trained with unconditional inputs, where the conditional and unconditional sample frequencies are controlled by their corresponding probabilities, i.e., p_c and p_u .

surpassed GANs on the image generation task and achieved both higher sample quality and better distribution coverage [4]. Its scalability further facilitates the building of large-scale text-to-image generation models [18, 22–24], which show marvelous image samples recently. The groundbreaking work of diffusion models is DDPM [9], which leverages the connection between Langevin dynamics [30] and denoising score matching [32] to build a weighted variational bound for optimization. However, the sampling process needs to follow the Markov chain step by step to produce one sample, which is extremely slow (e.g., usually 1000 or 4000 steps [4, 9]). DDIM [31] accelerates the sampling process via an iterative non-Markovian way while keeping the same training process unchanged. [19] further improves the log-likelihoods while maintaining high sample quality, and ADM [4] eventually outperforms GAN-based methods via an elaborately designed architecture and classifier guidance. Contemporarily, a cascaded diffusion model [10] is proposed with a sequence of lower resolution conditional diffusion models as an alternative approach to improve the sample fidelity and shows that conditional noisy augmentation is pivotal to the stacked architecture. Despite their findings and achievement in image synthesis, diffusion models on video generation have not been well-studied. Most recently, VDM [12] extends diffusion models to the video domain, which initiates the exploration of diffusion models on video generation. Specifically, they modify the 2D UNet to a spatial-temporal factorized 3D network and further present image-video joint training and gradient-based video extension techniques. MCVD [38] parameterizes unconditional video generation and conditional frame prediction

and interpolation models as a unified one by randomly dropping conditions (previous or future frames) during training, which shares the similar underneath idea with classifier-free guidance which joint trains a class-conditional and unconditional model. Make-A-Video [28], and Imagen Video [8] leverage a series of big diffusion models for large-scale video synthesis conditioned on a given text prompt. However, previous video-based video generation approaches all perform diffusion and denoising processes in pixel space, which requires substantial computational resources. In this paper, we extend the latent image diffusion model [23] to video by devising a 3D auto-encoder for video compression. Founded on this baseline, we further show how arbitrary long videos can be sampled via a hierarchical architecture and natural extensions of both conditional noise augmentation and classifier-free guidance to video generation.

3. Method

Fig. 2 shows our overall framework. We first compress video samples to a lower-dimensional latent space by a 3D autoencoder. Then we design a unified video diffusion model, which can perform both unconditional generation and conditional video prediction in one network, in the latent space. This enables our model to self-extend the generated video to an arbitrary length in an autoregressive way. To further improve the coherence of generated long video and alleviate the quality degradation problem caused by accumulated errors over time, we propose to first generate one video sparsely using an autoregressive model and then interpolate it to a higher frame rate by an interpolation diffusion

model.

3.1. Video Compression via a 3D Autoencoder

We compress videos using a lightweight 3D autoencoder, including an encoder \mathcal{E} and a decoder \mathcal{D} . Both of them consist of several layers of 3D convolutions. Formally, given a video sample $\mathbf{x}_0 \sim p_{data}(\mathbf{x}_0)$ where $\mathbf{x}_0 \in \mathbb{R}^{H \times W \times L \times 3}$, the encoder \mathcal{E} encodes it to its latent representation $\mathbf{z}_0 = \mathcal{E}(\mathbf{x}_0)$ where $\mathbf{z}_0 \in \mathbb{R}^{h \times w \times l \times c}$, $h = H/f_s$, $w = W/f_s$, and $l = L/f_t$. f_s and f_t are spatial and temporal down-sampling factors. The decoder \mathcal{D} decodes \mathbf{z}_0 to the reconstructed sample $\tilde{\mathbf{x}}_0$, i.e. $\tilde{\mathbf{x}}_0 = \mathcal{D}(\mathbf{z}_0)$. To ensure that the autoencoder is temporally shift-equivariant, we follow [6] to use repeat padding in all three-dimensional convolution kernels.

The training objective includes a reconstruction loss \mathcal{L}_{rec} and an adversarial loss \mathcal{L}_{adv} . The reconstruction loss \mathcal{L}_{rec} is comprised of a pixel-level mean-squared error (MSE) loss and a perceptual-level LPIPS [45] loss. The adversarial loss [5] is used to eliminate the blur in reconstruction usually caused by the pixel-level reconstruction loss and further improve the realism of the reconstruction. In summary, the overall training objective of \mathcal{E} and \mathcal{D} is

$$\mathcal{L}_{AE} = \min_{\mathcal{E}, \mathcal{D}} \max_{\psi} (\mathcal{L}_{rec}(\mathbf{x}_0, \mathcal{D}(\mathcal{E}(\mathbf{x}_0))) + \mathcal{L}_{adv}(\psi(\mathcal{D}(\mathcal{E}(\mathbf{x}_0))))). \quad (1)$$

where ψ is the discriminator used in adversarial training.

Our autoencoder is a vanilla auto-encoder without any KL or VQ regularization [23]. These two techniques are proposed to avoid an arbitrarily high-variance latent space in LDM [23]. For KL regularization, LDM rescales the latent by an estimated scale factor before performing diffusion model training, which, however, is vulnerable and has a great effect on generation performance (see Fig. 3 (a)). Imperfect scale factors could lead to implausible generation and bright spot artifacts when conducting experiments with different attention blocks (e.g., 3D attention block, see Fig. 3 (b)). We hypothesize that it is because a slight KL-regularization is not enough to reduce the variance of the latent space, and high-variance and center-shifted latent distribution harms the generation ability of diffusion models. Therefore we remove the KL regularization of the autoencoder during training and instead simply normalize the learned latent space with its post-computed mean μ and standard deviation σ after training, yielding $\mathbf{z}_0 \leftarrow (\mathbf{z}_0 - \mu)/\sigma$. We show in Fig. 3 that this process significantly improves the performance of latent diffusion models while the bright spot artifacts also disappear.

3.2. Short Video Generation

Revisiting Diffusion Models. We propose to perform diffusion and denoising on the video latent space. Given a

compressed latent code $\mathbf{z}_0 \sim p_{data}(\mathbf{z}_0)$, we train diffusion models to generate latent samples starting from a pure Gaussian noise $\mathbf{z}_T \sim \mathcal{N}(\mathbf{z}_T; \mathbf{0}, \mathbf{I})$ in T timesteps, producing a set of noisy latent variables, i.e., $\mathbf{z}_1, \dots, \mathbf{z}_T$. The forward diffusion process is gradually adding noise to \mathbf{z}_0 according to a predefined variance schedule β_1, \dots, β_T :

$$q(\mathbf{z}_{1:T}|\mathbf{z}_0) := \prod_{t=1}^T q(\mathbf{z}_t|\mathbf{z}_{t-1}), \quad (2)$$

$$q(\mathbf{z}_t|\mathbf{z}_{t-1}) := \mathcal{N}(\mathbf{z}_t; \sqrt{1 - \beta_t}\mathbf{z}_{t-1}, \beta_t\mathbf{I}). \quad (3)$$

Eventually, the data point \mathbf{z}_T becomes indistinguishable from pure Gaussian noise. To recover \mathbf{z}_0 from \mathbf{z}_T , diffusion models learn a backward process via

$$p_{\theta}(\mathbf{z}_{0:T}) := p(\mathbf{z}_T) \prod_{t=1}^T p_{\theta}(\mathbf{z}_{t-1}|\mathbf{z}_t), \quad (4)$$

$$p_{\theta}(\mathbf{z}_{t-1}|\mathbf{z}_t) := \mathcal{N}(\mathbf{z}_{t-1}; \mu_{\theta}(\mathbf{z}_t, t), \Sigma_{\theta}(\mathbf{z}_t, t)), \quad (5)$$

where θ is a parameterized neural network, typically a UNet commonly used in image synthesis, to predict $\mu_{\theta}(\mathbf{z}_t, t)$, and $\Sigma_{\theta}(\mathbf{z}_t, t)$. In practice, we parameterize $\mu_{\theta}(\mathbf{z}_t, t)$ by

$$\mu_{\theta}(\mathbf{z}_t, t) = \frac{1}{\sqrt{\alpha_t}} \left(\mathbf{z}_t - \frac{\beta_t}{\sqrt{1 - \alpha_t}} \epsilon_{\theta}(\mathbf{z}_t, t) \right), \quad (6)$$

where $\epsilon_{\theta}(\mathbf{z}_t, t)$ is eventually estimated, which is shown to work best [9]. We simply set $\Sigma_{\theta}(\mathbf{z}_t, t) = \beta_t^2 \mathbf{I}$ as in [9].

The training objective is a simplified version of variational bound:

$$\mathcal{L}_{simple}(\theta) := \|\epsilon_{\theta}(\mathbf{z}_t, t) - \epsilon\|_2^2, \quad (7)$$

where ϵ is drawn from a diagonal Gaussian distribution.

Video Generation Backbone. To model video samples in the 3D latent space, we follow [12] that exploits a spatial-temporal factorized 3D UNet architecture to estimate the ϵ . Specifically, we use space-only 3D convolution with the shape of $1 \times 3 \times 3$ and add temporal attention in partial layers. We investigate two kinds of attention: joint spatial-temporal multi-head self-attention and factorized space-time multi-head self-attention. We observe that applying the joint spatial-temporal attention does not exhibit significant benefit compared with the factorized one while increasing the model complexity and introducing spot-like artifacts in random locations sometimes (See Fig. 3). Thus we use factorized spatial-temporal attention as the default setting in our experiments. We use adaptive group normalization to inject the timestep embedding into normalization modules to control the channel-wise scale and bias parameters, which have also been demonstrated to be beneficial for improving sample fidelity in [4].

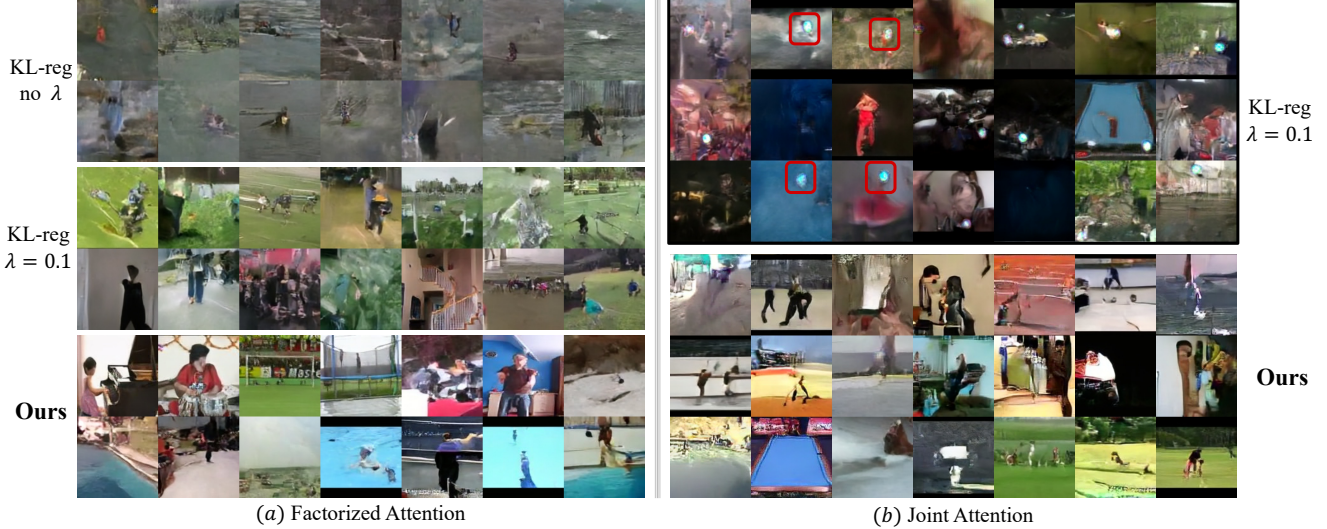


Figure 3. **Effect of latent-space normalization.** We discover that the generation performance is significantly affected by a hyperparameter: the scale factor imposed on latent codes when using a KL-regularized autoencoder (see (a)). An imperfect scale factor also induces obvious bright-spot artifacts when experimenting with different attention blocks (i.e., 3D attention block, see (b)). We remove the KL regularization and perform a normalization process on the latent space to make its distribution become mean 0 and variance 1, which largely improves the generation performance ((a) below) and avoids the bright-spot artifacts ((b) below). Comparisons in (a) and (b) are made with similar training epochs.

3.3. Long Video Generation

Autoregressive Video Generation. The aforementioned framework can only generate short videos, whose lengths are determined by the input frame number during training. We therefore propose a conditional latent diffusion model, which can produce future latent codes conditioned on the previous ones in an autoregressive manner, to facilitate long video generation. Considering a short clip latent $\mathbf{z}_t = \{\mathbf{z}_t^i\}_{i=1}^l$ where $\mathbf{z}_t^i \in \mathbb{R}^{h \times w \times c}$ and l is the number of latent codes within the clip, we can learn to predict future latent codes conditioned on the former ones. For each video frame in a clip latent, we add an additional binary map along the channel dimension to indicate whether it is a conditional frame or a frame to predict. Formally, given a binary clip $\mathbf{b} = \{\mathbf{b}^i\}_{i=1}^l$ where $\mathbf{b}^i \in \mathbb{R}^{h \times w \times 1}$, we obtain the conditional input clip as $\tilde{\mathbf{z}}_t = \{\tilde{\mathbf{z}}_t^i = [\mathbf{z}_t^i, \mathbf{b}^i]\}_{i=1}^l$ where $\tilde{\mathbf{z}}_t^i \in \mathbb{R}^{h \times w \times (c+1)}$. By randomly setting different binary maps to ones or zeros, we can train our diffusion model to perform both unconditional video generation and conditional video prediction jointly. Concretely, we set all maps in the binary clip \mathbf{b} to zeros for unconditional diffusion model training. For conditional video prediction, we set the first k binary maps $\{\mathbf{b}^i\}_{i=1}^k$ to ones and the remaining $\{\mathbf{b}^i\}_{i=k+1}^l$ to zeros. At the same time, we replace the first k latent codes with the ground truth, i.e. $\{\mathbf{z}_t^i\}_{i=1}^k \leftarrow \{\mathbf{z}_0^i\}_{i=1}^k$.

Hierarchical Video Generation. Generating videos in an autoregressive way has the risk of quality degradation caused by accumulated errors over time. We thus utilize a common strategy, hierarchical generation [3, 6, 13], to alle-

viate this problem. Specifically, we first train an autoregressive video generation model on sparse frames to form the basic storyline of the video and then train another interpolation model to fill the missing frames. The training of the interpolation model is similar to the autoregressive model, except that we set the binary maps of the middle frames between every two sparse frames to zeros.

Conditional Latent Perturbation. Although the above-mentioned hierarchical generation manner has demonstrated its effectiveness in prior works [6, 13], more prediction steps are indispensable to produce long-enough video samples. Thus, we propose conditional perturbation to mitigate the conditional error induced by the previous generation step. Specifically, rather than directly conditioning on \mathbf{z}_0 , we use the noisy latent code \mathbf{z}_s at an arbitrary time s , which could be computed by (3), as the condition during training, i.e., $\{\mathbf{z}_t^i\}_{i=1}^k \leftarrow \{\mathbf{z}_s^i\}_{i=1}^k$. This means we also perform a diffusion process on the conditional frames. To keep the conditional information preserved, a maximum threshold s_{max} is used to clamp the timesteps in a minor noise level. During sampling, a fixed noise level is used to consistently add noise during autoregressive prediction. Conditional latent perturbation is inspired by conditional noise augmentation, which has been proposed in cascaded diffusion models [10] to improve the performance of super-resolution diffusion models. While we extend it to video prediction, we are the first to demonstrate its effectiveness in producing long video samples.

4. Experiments

4.1. Experimental Setup

Datasets and Evaluation. We evaluate our method on UCF-101 [33], Sky Time-lapse [42], and Taichi [27]. We train all our models with the resolution of 256^2 on these datasets for unconditional video generation. The short clips used for training are selected with the frame stride of 1 at a random location of one video. For taichi, we select clips with the frame stride of 4 (i.e., skip three frames after selecting one) following prior work [6, 44] to make the human motion more dynamic. Due to the limited number of videos in UCF-101 and TaiChi, we adopt the full dataset for training. For the Sky Time-lapse dataset, we only train the model on its training split. All models are trained under the unconditional setting with no guidance information provided, such as class label. For quantitative evaluation, we report the commonly-used FVD [36] and KVD [37] for both short and long video generation. Specifically, we calculate FVD and KVD between 2048 real and fake videos with 16 frames, which we refer to FVD_{16} and KVD_{16} , for short video evaluation. All results for short video generation are calculated among 10 runs and report its mean and standard deviation. For long video evaluation, we estimate FVD and KVD among 512 samples in every non-overlapped 16-frame clip and report an FVD curve across 1024 frames calculated in 1 run, referred to as FVD_{1024} .

Baselines. We compared our approach with seven competing baselines, including GAN-based methods: TGAN-v2 [26], DiGAN [44], MoCoGAN-HD [34], and long-video GAN [2], autoregressive models TATS [6], and most recent diffusion-based models including Video Diffusion Models (VDM) [12] and MCVD [38]. Please note that VDM has mentioned in its main paper that it will not publish the source code. Thus we implement it by ourselves. Detailed implementations are documented in the supplement.

Implementation Details. We train the 3D autoencoder with the spatial and temporal downsampling factors of 8 and 4, respectively. The channel dimension of latent space is 4, which means a $256 \times 256 \times 16 \times 3$ video sample is encoded to a $32 \times 32 \times 4 \times 4$ latent. After the training of autoencoder, we fix its weights and then start to train an unconditional LVDM for short video generation. After that, the LVDM-prediction and LVDM-interpolation models are resumed from the unconditional one, starting the joint training with unconditional-conditional inputs, where the probabilities of unconditional and conditional inputs for the prediction model and interpolation model are (0.5, 0.5) and (0.1, 0.9), respectively. When synthesizing long videos, we use unconditional guidance with a scale equal to 0.1, and the noise level for conditional frames is set at 200 timesteps. Sampling is performed via DDPM standard denoising process unless otherwise specified. Most of our models are

Method	#Pixels	#Params	Step Time	FVD ₁₆ ↓	KVD ₁₆ ↓
VDM [12]	197k	445M (397+48)	4.9s (3.3+1.6)	1396	116
MCVD [38]	786k	441M	3s	2460	148
LVDM (Ours)	16k	437M (418+19)	0.8s	552	42

Table 1. Comparisons between our latent-space approach with two pixel-space approaches, VDM and MCVD, on unconditional short video generation (16 frames with the resolution of 256^2) on UCF-101. All models are trained with approximately the same parameters, the same training time (4.5 days), and the same devices (8 V100s). Batch sizes for all models are 16 except the video super-resolution model of VDM, which we set to 8 (the maximum number under limited GPU memory). + indicates two models needed. Our latent space-based method achieves better results in the setting of the same computational resources and the same training time.

trained on 8 or 32 A100 GPUs. More details are illustrated in supplementary materials.

4.2. Efficiency Comparison

To demonstrate the training and sampling efficiency of our method, we compare our approach with two pixel-space video diffusion models, including VDM [12] and MCVD [38] in Tab. 1 on the UCF-101 dataset. We implemented VDM with a base unconditional video diffusion model to synthesize videos of low resolution (16 frames with the resolution of 64^2) and a video super-resolution diffusion model to upscale the spatial resolution to 256^2 . We train MCVD following its official setting, except that we scale it to resolution 256^2 . Our method achieves better FVD than them when trained with a similar time and a similar number of model parameters.

4.3. Short Video Generation

Quantitative Results. In Tab. 2, we provide quantitative comparisons with previous methods on Sky-Timelapse, UCF-101, and Taichi, respectively. Our method outperforms previous state-of-the-art methods by a large margin. Specifically, on the Sky-Timelapse dataset, we reduce FVD from 116.5 to 95.18 under the resolution of 256^2 . In addition, our high-resolution performance also surpasses those of the state-of-the-art methods in FVD under the resolution of 128^2 . On the UCF-101 and taichi datasets, we achieve new state-of-the-art results under the resolution of 256^2 , while our FVD is comparable to the best result under the resolution of 128^2 . LVDM outperforms diffusion-based method MCVD on UCF-101 regarding both scores and resolution.

Qualitative Results. In Fig. 4, we showcase visual comparisons with DiGAN [44] and TATS [6]. We observe that samples produced by DiGAN exhibit coordinates-like artifacts in many samples, TATS tends to generate samples with flat contents and lacks diversity, while our LVDM can synthesize video samples with high fidelity and diversity. More

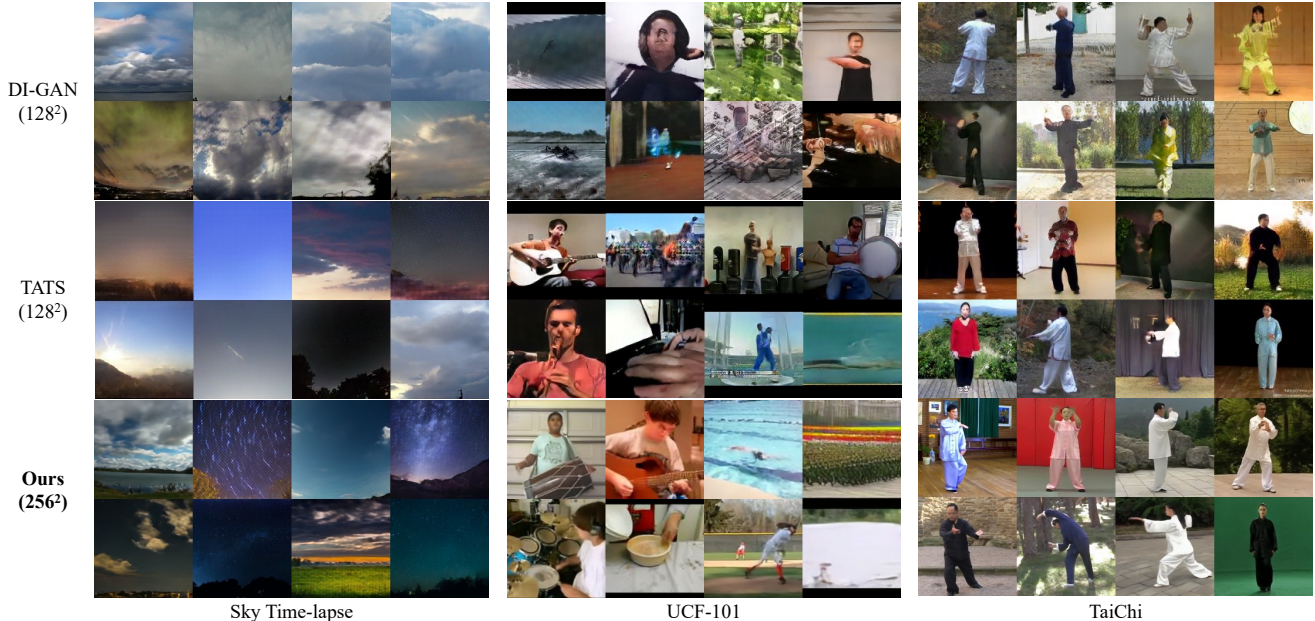


Figure 4. Qualitative comparison on unconditional short video generation (16 frames) on UCF-101 [33] Sky Time-lapse [42], and TaiChi [27]. We showcase results including DIGAN [44], TATS [6], and LVDM (Ours). LVDM can generate videos with 16 frames simultaneously under 256^2 resolution and achieves higher resolution while better quality results (Zoom in for better view). Samples of baseline methods are obtained from their official checkpoints. All frames shown are selected at $t = 10$ from eight randomly generated samples.

Method	FVD ₁₆ ↓	KVD ₁₆ ↓
<i>Resolution 128²</i>		
MoCoGAN-HD [34]	183.6 ± 5.2	13.9 ± 0.7
DIGAN [44]	114.6 ± 4.9	6.8 ± 0.5
TATS [6]	132.6 ± 2.6	5.7 ± 0.3
Long-video GAN [6]	107.5	-
<i>Resolution 256²</i>		
Long-video GAN [6]	116.5	-
LVDM (Ours)	95.2 ± 2.3	3.9 ± 0.1

(a) Sky Time-lapse

Method	FVD ₁₆ ↓	KVD ₁₆ ↓
<i>Resolution 64²</i>		
MCVD [38]	1143	-
<i>Resolution 128²</i>		
TGAN-v2 [26]	1209 ± 28	-
DIGAN [44]	577 ± 21	-
TATS [6]	420 ± 18	-
<i>Resolution 256²</i>		
MoCoGAN-HD* [34]	700 ± 24	-
TATS [6]	635 ± 34	55 ± 5
LVDM (Ours)	372 ± 11	27 ± 1

(b) UCF-101

Method	FVD ₁₆ ↓	KVD ₁₆ ↓
<i>Resolution 128²</i>		
MoCoGAN-HD [34]	144.7 ± 6.0	25.4 ± 1.9
DIGAN [44]	128.1 ± 4.9	20.6 ± 1.1
TATS [6]	94.6 ± 2.7	9.8 ± 1.0
<i>Resolution 256²</i>		
DIGAN [44]	156.7 ± 6.2	-
LVDM (Ours)	99.0 ± 2.6	15.3 ± 0.9

(c) TaiChi

Table 2. Quantitative results of short video generation on three datasets.

comparisons are documented in supplementary materials.

4.4. Long Video Generation

We compare our method LVDM with TATS [6] for long video generation with 1024 frames on the UCF-101 and Sky Time-lapse datasets. Both LVDM and TATS experiment with a pure autoregressive prediction model (autoregressive) and a combination of a prediction model with an interpolation model (hierarchical). Fig. 5 and Fig. 6 present the qualitative and quantitative comparison results, respectively. Note that TATS does not provide its hierarchical checkpoints on UCF-101. On the Sky Time-lapse, we compare two methods under a hierarchical setting.

Our method achieves both lower FVD scores and slower quality degradation over time compared with TATS. Specif-

ically, on challenging UCF-101, our LVDM-autoregressive has much slower quality degradation over time compared with TATS-autoregressive. Our LVDM-hierarchical further significantly alleviates the quality degradation problem. On Sky Timelapse, both two hierarchical-based approaches achieve minor quality degradation over time, while our methods have better FVD scores.

4.5. Ablation Study

Latent Space Normalization. In Tab. 3, we show FVD and KVD results of different scale factors (λ) and our latent space normalization to demonstrate its effectiveness. All the results are evaluated with 100 DDIM timesteps. Our latent space normalization significantly improves the generation results, while we do not need any extra regularizations



Figure 5. Qualitative results of generated long videos compared with state-of-the-art approach TATS [6] on UCF-101. Each frame is selected with a frame step 16. Both approaches are compared in the autoregressive setting.

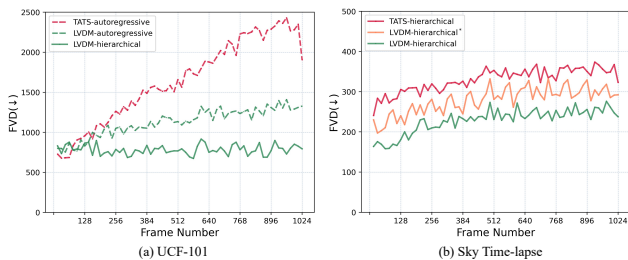


Figure 6. Quantitative comparison with TATS on long video generation (1024 frames) on the UCF-101 and Sky Time-lapse datasets. Note that our method renders long videos at the 256^2 resolution, while videos produced by TATS are at the 128^2 resolution. LVDM outperforms TATS in both autoregressive and hierarchical manners. * indicates DDIM sampling with 100 timesteps.

Method	FVD ₁₆ ↓	KVD ₁₆ ↓
$\lambda=1$	2111±43	150±5
$\lambda=0.26$	1304±29	93±5
$\lambda=0.1$	1869±50	136±6
Ours	791±24	64±4

Table 3. Results of different λ values and latent space normalization (Ours). we restrict the training time to 500 epochs for all models.

for the autoencoder and the hyperparameter λ .

Conditional Latent Perturbation. Fig. 7 shows the ablation results of conditional latent perturbation. We can observe that it can slow down the performance degradation trend, especially when the frame number is larger than 512, demonstrating its effectiveness on long video generation.

Unconditional Guidance. We also explore *unconditional guidance* attempting to alleviate quality degradation of autoregressive generation by leveraging the unconditional score to guide the autoregressive conditional generation with a guidance strength, *i.e.*, $\tilde{\epsilon}_\theta = (1+w)\epsilon_c - w\epsilon_u$ [11]. This techniques works well on Sky Time-lapse but harms the FVD performance on UCF-101 as shown in Fig. 8.

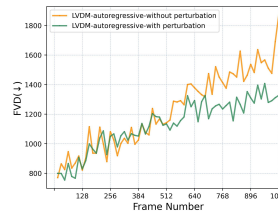


Figure 7. Ablation study of conditional latent perturbation on long video generation (1024 frames) on UCF-101.

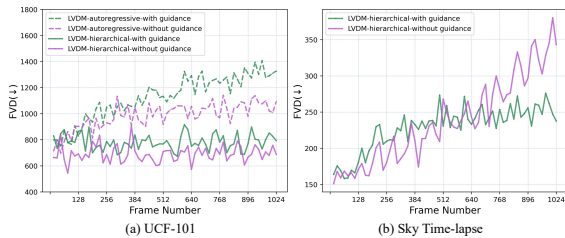


Figure 8. Effect of unconditional guidance. It works well on Sky Time-lapse but harms the FVD on UCF-101.

5. Conclusion

In this work, we devise an efficient DM-based framework for video generation, which significantly reduces the data dimension and speeds up the training and sampling. Our novel framework is a joint framework for both unconditional and conditional video synthesis (*i.e.*, prediction and infilling). With its better modeling capacity, we achieve new state-of-the-art results and higher resolution on various datasets under short and long video generation settings. We further demonstrate the effectiveness of conditional latent perturbation in reducing the accumulated error induced during autoregressively extending video lengths. We hope our method will serve as a strong baseline for future video generation works. Future explorations could be made regarding better architecture design choices and further speeding up the training and sampling of video diffusion models.

References

- [1] Andrew Brock, Jeff Donahue, and Karen Simonyan. Large scale GAN training for high fidelity natural image synthesis. In *ICLR*, 2019. 1
- [2] Tim Brooks, Janne Hellsten, Miika Aittala, Ting-Chun Wang, Timo Aila, Jaakko Lehtinen, Ming-Yu Liu, Alexei A Efros, and Tero Karras. Generating long videos of dynamic scenes. *arXiv preprint arXiv:2206.03429*, 2022. 1, 6
- [3] Lluís Castrejón, Nicolas Ballas, and Aaron Courville. Hierarchical video generation for complex data. *arXiv preprint arXiv:2106.02719*, 2021. 5
- [4] Prafulla Dhariwal and Alexander Nichol. Diffusion models beat gans on image synthesis. *Advances in Neural Information Processing Systems*, 34:8780–8794, 2021. 1, 3, 4
- [5] Patrick Esser, Robin Rombach, and Bjorn Ommer. Taming transformers for high-resolution image synthesis. In *Proceedings of the IEEE/CVF conference on computer vision and pattern recognition*, pages 12873–12883, 2021. 1, 2, 4
- [6] Songwei Ge, Thomas Hayes, Harry Yang, Xi Yin, Guan Pang, David Jacobs, Jia-Bin Huang, and Devi Parikh. Long video generation with time-agnostic vqgan and time-sensitive transformer. *arXiv preprint arXiv:2204.03638*, 2022. 1, 2, 4, 5, 6, 7, 8
- [7] Jiawei He, Andreas Lehrmann, Joseph Marino, Greg Mori, and Leonid Sigal. Probabilistic video generation using holistic attribute control. In *Proceedings of the European Conference on Computer Vision (ECCV)*, pages 452–467, 2018. 1, 2
- [8] Jonathan Ho, William Chan, Chitwan Saharia, Jay Whang, Ruiqi Gao, Alexey Gritsenko, Diederik P Kingma, Ben Poole, Mohammad Norouzi, David J Fleet, et al. Imagen video: High definition video generation with diffusion models. *arXiv preprint arXiv:2210.02303*, 2022. 3
- [9] Jonathan Ho, Ajay Jain, and Pieter Abbeel. Denoising diffusion probabilistic models. *Advances in Neural Information Processing Systems*, 33:6840–6851, 2020. 1, 3, 4
- [10] Jonathan Ho, Chitwan Saharia, William Chan, David J Fleet, Mohammad Norouzi, and Tim Salimans. Cascaded diffusion models for high fidelity image generation. *J. Mach. Learn. Res.*, 23:47–1, 2022. 3, 5
- [11] Jonathan Ho and Tim Salimans. Classifier-free diffusion guidance. *arXiv preprint arXiv:2207.12598*, 2022. 8
- [12] Jonathan Ho, Tim Salimans, Alexey Gritsenko, William Chan, Mohammad Norouzi, and David J Fleet. Video diffusion models. *arXiv preprint arXiv:2204.03458*, 2022. 1, 3, 4, 6
- [13] Wenyi Hong, Ming Ding, Wendi Zheng, Xinghan Liu, and Jie Tang. Cogvideo: Large-scale pretraining for text-to-video generation via transformers. *arXiv preprint arXiv:2205.15868*, 2022. 5
- [14] Tero Karras, Miika Aittala, Samuli Laine, Erik Härkönen, Janne Hellsten, Jaakko Lehtinen, and Timo Aila. Alias-free generative adversarial networks. In *NeurIPS*, 2021. 1
- [15] Tero Karras, Samuli Laine, and Timo Aila. A style-based generator architecture for generative adversarial networks. In *CVPR*, 2019. 1
- [16] Tero Karras, Samuli Laine, Miika Aittala, Janne Hellsten, Jaakko Lehtinen, and Timo Aila. Analyzing and improving the image quality of StyleGAN. In *CVPR*, 2020. 1
- [17] Manoj Kumar, Mohammad Babaeizadeh, Dumitru Erhan, Chelsea Finn, Sergey Levine, Laurent Dinh, and Durk Kingma. Videoflow: A conditional flow-based model for stochastic video generation. *arXiv preprint arXiv:1903.01434*, 2019. 1, 2
- [18] Alex Nichol, Prafulla Dhariwal, Aditya Ramesh, Pranav Shyam, Pamela Mishkin, Bob McGrew, Ilya Sutskever, and Mark Chen. Glide: Towards photorealistic image generation and editing with text-guided diffusion models. *arXiv preprint arXiv:2112.10741*, 2021. 1, 3
- [19] Alexander Quinn Nichol and Prafulla Dhariwal. Improved denoising diffusion probabilistic models. In *International Conference on Machine Learning*, pages 8162–8171. PMLR, 2021. 3
- [20] Aaron van den Oord, Oriol Vinyals, and Koray Kavukcuoglu. Neural discrete representation learning. *arXiv preprint arXiv:1711.00937*, 2017. 2
- [21] Ruslan Rakhimov, Denis Volkhonskiy, Alexey Artemov, Denis Zorin, and Evgeny Burnaev. Latent video transformer. *arXiv preprint arXiv:2006.10704*, 2020. 1
- [22] Aditya Ramesh, Prafulla Dhariwal, Alex Nichol, Casey Chu, and Mark Chen. Hierarchical text-conditional image generation with clip latents. *arXiv preprint arXiv:2204.06125*, 2022. 1, 3
- [23] Robin Rombach, Andreas Blattmann, Dominik Lorenz, Patrick Esser, and Björn Ommer. High-resolution image synthesis with latent diffusion models. In *Proceedings of the IEEE/CVF Conference on Computer Vision and Pattern Recognition*, pages 10684–10695, 2022. 1, 3, 4
- [24] Chitwan Saharia, William Chan, Saurabh Saxena, Lala Li, Jay Whang, Emily Denton, Seyed Kamyar Seyed Ghasemipour, Burcu Karagol Ayan, S Sara Mahdavi, Rapha Gontijo Lopes, et al. Photorealistic text-to-image diffusion models with deep language understanding. *arXiv preprint arXiv:2205.11487*, 2022. 1, 3
- [25] Masaki Saito, Eiichi Matsumoto, and Shunta Saito. Temporal generative adversarial nets with singular value clipping. In *Proceedings of the IEEE international conference on computer vision*, pages 2830–2839, 2017. 1, 2
- [26] Masaki Saito, Shunta Saito, Masanori Koyama, and Sotuke Kobayashi. Train sparsely, generate densely: Memory-efficient unsupervised training of high-resolution temporal gan. *International Journal of Computer Vision*, 128:2586–2606, 2020. 1, 2, 6, 7
- [27] Aliaksandr Siarohin, Stéphane Lathuilière, Sergey Tulyakov, Elisa Ricci, and Nicu Sebe. First order motion model for image animation. *NeurIPS*, 2019. 6, 7
- [28] Uriel Singer, Adam Polyak, Thomas Hayes, Xi Yin, Jie An, Songyang Zhang, Qiyuan Hu, Harry Yang, Oron Ashual, Oran Gafni, et al. Make-a-video: Text-to-video generation without text-video data. *arXiv preprint arXiv:2209.14792*, 2022. 3
- [29] Ivan Skorokhodov, Sergey Tulyakov, and Mohamed Elhoseiny. Stylegan-v: A continuous video generator with the

- price, image quality and perks of stylegan2. In *Proceedings of the IEEE/CVF Conference on Computer Vision and Pattern Recognition*, pages 3626–3636, 2022. 1, 2
- [30] Jascha Sohl-Dickstein, Eric Weiss, Niru Maheswaranathan, and Surya Ganguli. Deep unsupervised learning using nonequilibrium thermodynamics. In *International Conference on Machine Learning*, pages 2256–2265. PMLR, 2015. 3
- [31] Jiaming Song, Chenlin Meng, and Stefano Ermon. Denoising diffusion implicit models. *arXiv preprint arXiv:2010.02502*, 2020. 3
- [32] Yang Song, Jascha Sohl-Dickstein, Diederik P Kingma, Abhishek Kumar, Stefano Ermon, and Ben Poole. Score-based generative modeling through stochastic differential equations. *arXiv preprint arXiv:2011.13456*, 2020. 3
- [33] Khurram Soomro, Amir Roshan Zamir, and Mubarak Shah. Ucf101: A dataset of 101 human actions classes from videos in the wild. *arXiv preprint arXiv:1212.0402*, 2012. 2, 6, 7
- [34] Yu Tian, Jian Ren, Menglei Chai, Kyle Olszewski, Xi Peng, Dimitris N. Metaxas, and Sergey Tulyakov. A good image generator is what you need for high-resolution video synthesis. In *International Conference on Learning Representations*, 2021. 1, 2, 6, 7
- [35] Sergey Tulyakov, Ming-Yu Liu, Xiaodong Yang, and Jan Kautz. Mocogan: Decomposing motion and content for video generation. In *Proceedings of the IEEE conference on computer vision and pattern recognition*, pages 1526–1535, 2018. 1, 2
- [36] Thomas Unterthiner, Sjoerd van Steenkiste, Karol Kurach, Raphael Marinier, Marcin Michalski, and Sylvain Gelly. Towards accurate generative models of video: A new metric & challenges. *arXiv preprint arXiv:1812.01717*, 2018. 6
- [37] Thomas Unterthiner, Sjoerd van Steenkiste, Karol Kurach, Raphael Marinier, Marcin Michalski, and Sylvain Gelly. Towards accurate generative models of video: A new metric & challenges. *ICLR*, 2019. 6
- [38] Vikram Voleti, Alexia Jolicoeur-Martineau, and Christopher Pal. Masked conditional video diffusion for prediction, generation, and interpolation. *arXiv preprint arXiv:2205.09853*, 2022. 1, 3, 6, 7
- [39] Carl Vondrick, Hamed Pirsiavash, and Antonio Torralba. Generating videos with scene dynamics. *Advances in neural information processing systems*, 29, 2016. 1, 2
- [40] Jacob Walker, Ali Razavi, and Aäron van den Oord. Predicting video with vqvae. *arXiv preprint arXiv:2103.01950*, 2021. 2
- [41] Dirk Weissenborn, Oscar Täckström, and Jakob Uszkoreit. Scaling autoregressive video models. *arXiv preprint arXiv:1906.02634*, 2019. 1
- [42] Wei Xiong, Wenhan Luo, Lin Ma, Wei Liu, and Jiebo Luo. Learning to generate time-lapse videos using multi-stage dynamic generative adversarial networks. In *The IEEE Conference on Computer Vision and Pattern Recognition (CVPR)*, June 2018. 2, 6, 7
- [43] Wilson Yan, Yunzhi Zhang, Pieter Abbeel, and Aravind Srinivas. Videogpt: Video generation using vq-vae and transformers. *arXiv preprint arXiv:2104.10157*, 2021. 1, 2
- [44] Sihyun Yu, Jihoon Tack, Sangwoo Mo, Hyunsu Kim, Junho Kim, Jung-Woo Ha, and Jinwoo Shin. Generating videos with dynamics-aware implicit generative adversarial networks. In *International Conference on Learning Representations*, 2022. 1, 2, 6, 7
- [45] Richard Zhang, Phillip Isola, Alexei A Efros, Eli Shechtman, and Oliver Wang. The unreasonable effectiveness of deep features as a perceptual metric. In *CVPR*, 2018. 4